Interaction forces and adhesion of supported myelin lipid bilayers modulated by myelin basic protein

Younjin Min[a], Kai Kristiansen[a], Joan M. Boggs[b,c], Cynthia Husted[a], Joseph A. Zasadzinski[a], and Jacob Israelachvili[a,1]

[a]Department of Chemical Engineering, University of California, Santa Barbara, CA 93106; [b]Department of Molecular Structure and Function, The Hospital for Sick Children, Toronto, ON, Canada M5G 1X8; and [c]Department of Laboratory Medicine and Pathobiology, University of Toronto, Toronto, ON, Canada M5G 1L5

Contributed by Jacob Israelachvili, December 23, 2008 (sent for review September 26, 2008)

Force–distance measurements between supported lipid bilayers mimicking the cytoplasmic surface of myelin at various surface coverages of myelin basic protein (MBP) indicate that maximum adhesion and minimum cytoplasmic spacing occur when each negative lipid in the membrane can bind to a positive arginine or lysine group on MBP. At the optimal lipid/protein ratio, additional attractive forces are provided by hydrophobic, van der Waals, and weak dipolar interactions between zwitterionic groups on the lipids and MBP. When MBP is depleted, the adhesion decreases and the cytoplasmic space swells; when MBP is in excess, the bilayers swell even more. Excess MBP forms a weak gel between the surfaces, which collapses on compression. The organization and proper functioning of myelin can be understood in terms of physical noncovalent forces that are optimized at a particular combination of both the amounts of and ratio between the charged lipids and MBP. Thus loss of adhesion, possibly contributing to demyelination, can be brought about by either an excess or deficit of MBP or anionic lipids.

biomembrane adhesion | lipid–protein interactions | multiple sclerosis | myelin membrane structure | experimental allergic encephalomyelitis

The myelin sheath is a multilamellar membrane surrounding the axons of neurons in both the central nervous system (CNS) and peripheral nervous system (PNS) (1) as shown in Fig. 1 *A* and *B*. The myelin sheath consists of repeating units of double bilayers separated by 3- to 4-nm-thick aqueous layers that alternate between the cytoplasmic and extracellular faces of cell membranes (2) (Fig. 1*C*). Dehydrated myelin is unusual in that it is composed of 75–80% lipid and 20–25% protein by weight, compared with ≈50% of most other cell membranes (3) (Fig. 1 *C* and *D*). Multiple lipids make up the myelin sheath (Table 1), and each sheath, with its own distinct physical properties, contributes to the structure, adhesive stability, and possibly the pathogenesis of the myelin membrane. The asymmetric distribution of lipid composition on the cytoplasmic and extracellular faces likely also plays an important role (4). Myelin basic protein (MBP) constitutes 20–30% of total protein by weight and is located only between the 2 cytoplasmic faces, where it acts as an intermembrane adhesion protein.

The myelin sheath acts as an electrical insulator, forming a capacitor surrounding the axon, which allows for faster and more efficient conduction of nerve impulses than unmyelinated nerves (5). According to cable theory, the time to transmit a signal over a distance x is $\tau = \frac{1}{2}RC_{\text{myelin}}x^2$, where R is the resistance per unit length, and C_{myelin} is the capacitance between the axon and its surroundings, which is given by (5)

$$C_{\text{myelin}} = \frac{2\pi\varepsilon_0\varepsilon_{\text{myelin}}}{\log(R_O/R_I)} \text{ per unit length,} \qquad [1]$$

where R_O and R_I are the outer and inner radii (Fig. 1*B*), ε_0 is the permittivity of free space, and the mean dielectric constant of the myelin sheath is

$$\varepsilon_{\text{myelin}} = [2\varepsilon_{hc}D_B + \varepsilon_P D_P + \varepsilon_W(D_I + D_O)]/D_{\text{Tot}}, \qquad [2]$$

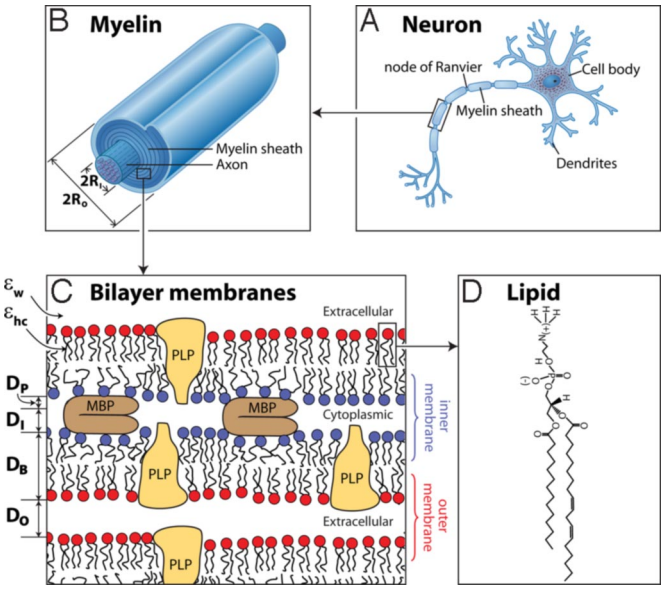

Fig. 1. The structure of the myelin sheath. The myelinated axon (*A*), myelin sheath (*B*), bilayer membranes (*C*), and phosphatidylethanolamine (PE) (*D*) are shown. Each bilayer of thickness D_B is separated by cytoplasmic and extracellular water gaps of thicknesses D_I and D_O and effective protein thickness D_P occupied by the fraction of MBP constituting the cytoplasmic water gap.

where $D_{\text{Tot}} = [2D_B + D_I + D_P + D_O]$ (Fig. 1*C*). Low capacitance necessitates a low value of $\varepsilon_{\text{myelin}}$, which is promoted by the much lower dielectric constants of the lipid chains ($\varepsilon_{hc} \approx 2$) and proteins ($\varepsilon_P = 2.5$–$4.0$) (6) compared with that of water ($\varepsilon_w \approx 80$ for bulk water and $\varepsilon_w \approx 40$ for "interfacial" or "partially trapped" water in thin films) (7). Increasing the thickness of the myelin sheath increases R_O/R_I, and tighter membrane binding within the sheath decreases the water gaps, both of which decrease C_{myelin}. For squid axon, a measured value of $\varepsilon_{\text{myelin}} \approx 8.5$ has been reported (8). Inserting the following measured or estimated values into Eq. **2**: $\varepsilon_P = 2.5$–4.0 (6), $D_B \approx 4.5$ nm, $D_O \approx 3$ nm, $D_I \approx D_P \approx 1$ nm (assuming 50% of the cytoplasmic gap is protein) (1), and $\varepsilon_w \approx 40$ (7), we obtain $\varepsilon_{\text{myelin}} \approx 13$, which is close to the measured value.

Myelin dysfunctions vary from deterioration of signal transduction to demyelinating diseases such as multiple sclerosis (MS) (3). MS is characterized by the appearance of lesions, reflecting loss of membrane adhesion, swelling across the water gaps, vacuolization, vesiculation, and eventual disintegration of the

Author contributions: Y.M., K.K., J.A.Z., and J.I. designed research; Y.M. and K.K. performed research; J.M.B. and C.H. contributed new reagents/analytic tools; Y.M., K.K., and J.I. analyzed data; and Y.M., K.K., J.M.B., C.H., J.A.Z., and J.I. wrote the paper.

The authors declare no conflict of interest.

[1]To whom correspondence should be addressed. E-mail: jacob@engineering.ucsb.edu.

Table 1. Lipid compositions of healthy and diseased bilayers calculated as mole % of lipid in the extracellular (EXT) and cytoplasmic (CYT) faces of myelin membranes

	Healthy				EAE			
Lipid type (i)	EXT, X_i^{EXT}	CYT, X_i^{CYT}	Bilayer, X_i^{TOT}	CYT, x_i^{CYT}	EXT, X_i^{EXT}	CYT, X_i^{CYT}	Bilayer, X^{TOT}	CYT, x_i^{CYT} *
Cholesterol (CHOL)	22.4	10.6	32.9	31.6	25.8	12.1	37.9	37.4
Phosphatidylserine (PS^-)	0.7	2.4	3.1	7.0	4.7	2.4	7.1	7.4
Hydroxylated cerebrosides (HCER)	13.9	0	13.9	0	14.7	0	14.7	0
Nonhydroxylated cerebrosides (NCER)	2.3	0	2.3	0	2.4	0	2.4	0
Cerebroside sulfatide ($SCER^-$)	6.4	0	6.4	0	3.8	0	3.8	0
Sphingomyelin (SM ±)	2.8	2.1	4.9	6.2	0.9	0.7	1.6	2.2
Phosphatidylcholine (PC ±)	12.1	8.7	20.8	25.9	8.9	6.5	15.4	20.1
Phosphatidylethanolamine (PE ±)	6.0	9.7	15.7	29.0	6.5	10.6	17.1	32.9
Total mole %, ΣX_i and Σx_i	66.5	33.5	100	100	67.8	32.2	100	100

X_i^{TOT} is the total mole fraction (percent of lipid of type i, so that $\Sigma_i X_i^{TOT} = 100\%$. X_i^{EXT} and X_i^{CYT} are the total mole fractions of lipid of type i in the extracellular and cytoplasmic faces, so that $X_i^{TOT} = X_i^{EXT} + X_i^{CYT}$, and $\Sigma_i X_i^{TOT} = \Sigma_i X_i^{EXT} + \Sigma_i X_i^{CYT} = 100\%$. x_i^{CYT} are the mole fractions of lipid of type i in the cytoplasmic faces only, so that $\Sigma_i x_i^{CYT} = 100\%$. The x_i and X_i values are related by $x_i^{CYT} = 100X_i^{CYT}/\Sigma_i X_i^{CYT}$. We may note that the total mole fraction of lipids in the extracellular faces $\Sigma_i X_i^{EXT}$ is typically twice that for the cytoplasmic lipids $\Sigma_i X_i^{CYT}$ (see bottom row). The ''missing'' volume is likely taken up by the MBP in the cytoplasmic spaces. Myelin membranes are from marmoset white matter (10).

*These compositions were used in the experiments.

myelin structure (9). It has been shown in previous work that in experimental allergic encephalomyelitis (EAE) in the common marmoset—an established animal model for MS (10)—the lipid composition changes, in particular the ratios of charged to uncharged lipids (Table 1). In other studies, both the charged lipid and MBP isomer composition and the balance (relative amounts) between the charged lipid and MBP isomer composition change in MS and EAE tissues (11, 12). We show here that either an excess or a deficit of MBP relative to anionic lipids affects the interactions between myelin membranes across the cytoplasmic space, although we note that whether swelling and demyelination occur at both the extracellular and cytoplasmic spaces during MS has not yet been established.

Many attempts (10, 13, 14) have been made to experimentally observe the molecular interactions (forces) between myelin lipids and MBP. However, no techniques have quantified how electrostatic interactions (namely, double-layer, coulombic or ionic bonds, and salt bridges), which can be attractive or repulsive, and attractive van der Waals and hydrophobic interactions act across the cytoplasmic and extracellular spaces of myelin to ensure the integrity of its structure. The aim of this study was to measure these forces, especially the adhesion forces, of reconstituted myelin membranes at different lipid/protein ratios to establish the correlations between membrane composition, structure, interaction forces, and ultimate function.

To determine whether changes in the lipid or MBP concentration or mole fraction affect the adhesion of the cytoplasmic faces of the myelin sheath, we compared the forces between model bilayers of lipid mixtures that reflect the composition of EAE myelin in the common marmoset and of normal, healthy myelin (10, 14). Model membranes with the composition of the cytoplasmic side of EAE myelin (see Table 1) were constructed on mica surfaces by Langmuir–Blodgett (LB) deposition, and the forces between the membranes were measured by using a surface forces apparatus (SFA) after exposure to various solution concentrations of MBP. Physical–chemical studies of the interaction of MBP with myelin lipids have confirmed that the attraction between MBP and lipid is largely electrostatic (15): There are ≈20 ± 3 anionic lipid molecules per molecule of MBP in healthy myelin (15). In addition, there is good evidence that the hydrophobic segments that make up ≈25% of MBP (3, 15) interact with the hydrophobic lipid chains either by partially penetrating into the bilayers (16) or by expanding the bilayers (14, 15). These lipid–protein interactions also affect the intramembrane forces that determine the fluidity and mobility of the lipids and proteins within the membranes (3) and the formation of compositionally distinct domains (17).

Results

SFA Force–Distance Measurements. Fig. 2 shows the long- (*A*) and short- (*B*) range forces measured between EAE cytoplasmic bilayers in the absence and presence of various amounts of MBP. Fig. 2*A* is a semilog plot showing the strongly repulsive forces on approach, and Fig. 2*B* is a linear plot showing the weak (negative) adhesion forces[†] on separation as a function of bulk MBP concentration.

To relate the measured adhesive forces to the surface coverage rather than the bulk solution concentration of MBP,[‡] we have separately measured the surface coverage at each concentration. The same fringes-of-equal-chromatic-order (FECO) optical technique (18) used to measure the distance between mica surfaces can be used to determine the refractive index $n(D)$ of the aqueous space between the bilayers, which can then be used to estimate the surface coverage of MBP. Because in a first approximation, $n^2(D)$ is a linear function of the volume fraction ϕ_i of each component i, $n(D)$ is given by (19)

$$n^2(D) = \sum \phi_i n_i^2 = \phi_w n_w^2 + \phi_B n_B^2 + \phi_{MBP} n_{MBP}^2, \qquad [3]$$

where $\sum \phi_i = 1$ and subscripts w, B, and MBP denote water, bilayer, and MBP, respectively.

In the absence of MBP ($\phi_{MBP} = 0$), Eq. **3** reduces to $n^2(D) = \phi_w n_w^2 + \phi_B n_B^2$. In this case, $\phi_w = D_w/D$ and $\phi_B = (1 - \phi_w) = 2D_B/D$, and we have:

$$n^2(D) = n_w^2 + \frac{2D_B}{D}(n_B^2 - n_w^2), \qquad [4]$$

where $D = 2D_B + D_w$ is the total mica–mica gap thickness and $n_w = 1.333$. Thus, by plotting $n^2(D) - n_w^2$ as a function of $(n_B^2 - n_w^2)/D$, we can determine $2D_B$ and ϕ_B. This analysis gives $2D_B \approx 7.4$ nm by using $n_B = 1.47$.

[†]Negative (adhesion) forces cannot be displayed on log plots.

[‡]Most of the MBP injected into the solution ends up on the negatively charged surfaces; i.e., there is an equilibrium distribution of MBP molecules between those molecules that are the bulk and those molecules adsorbed on the surfaces, which is strongly biased in the direction of the surfaces. From the concentration giving rise to monolayer coverage, the equilibrium affinity or association constant is estimated to be 10^{-9} M, which is typical of antibody–antigen and ligand–receptor bonds.

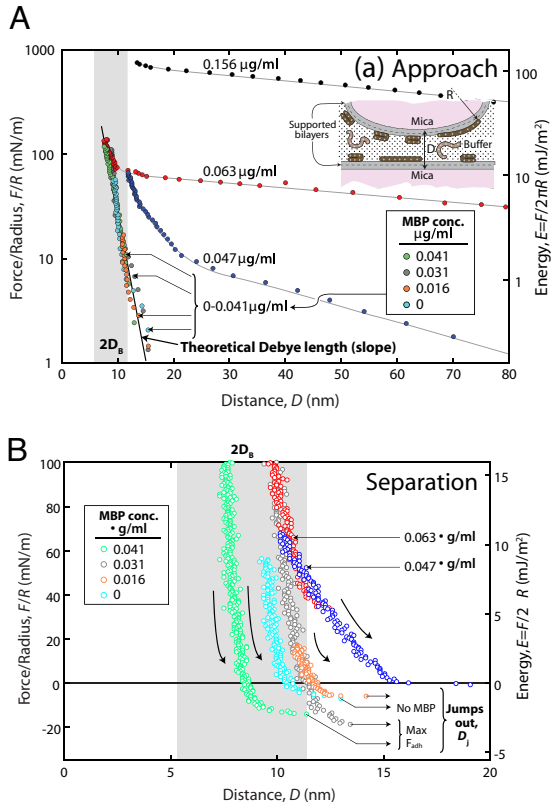

Fig. 2. Normalized force–distance profiles with different amounts of MBP in solution. $F(D)/R$ measured on approach (*A*) and on separation (*B*) between 2 EAE cytoplasmic myelin bilayers in the presence of various amounts of MBP (in μg of injected MBP into the 80-mL incubating Mops buffer solution) at pH 7.2 and 24 °C. $D = 0$ corresponds to mica–mica contact, and D_B represents 1 bilayer thickness as defined in Fig. 1. The right axis shows the corresponding interaction energy, $E(D) = F(D)/2\pi R$, per unit area between 2 planar bilayers, calculated according to the Derjaguin approximation (23). The equilibrium separation between planar bilayers corresponds to where F/R is a minimum; zero force in *B* is the equilibrium separation between 2 curved surfaces. Configuration of MBP in the bulk is primarily random coil (26, 37), which transforms into a C-shaped structure when it interacts with (bridges) 2 bilayers (38). Each curve corresponds to the second approach–separation cycle (compare Fig. 4). The numbers shown are the bulk MBP concentrations; the boxed concentrations refer only to the 4 curves in the concentration range 0–0.041 μg/mL, which have matching colored data points. The range of $2D_B$ was obtained by subtracting the water layer thickness of $D_W \approx$ 2 nm from final "hard wall contact" distances.

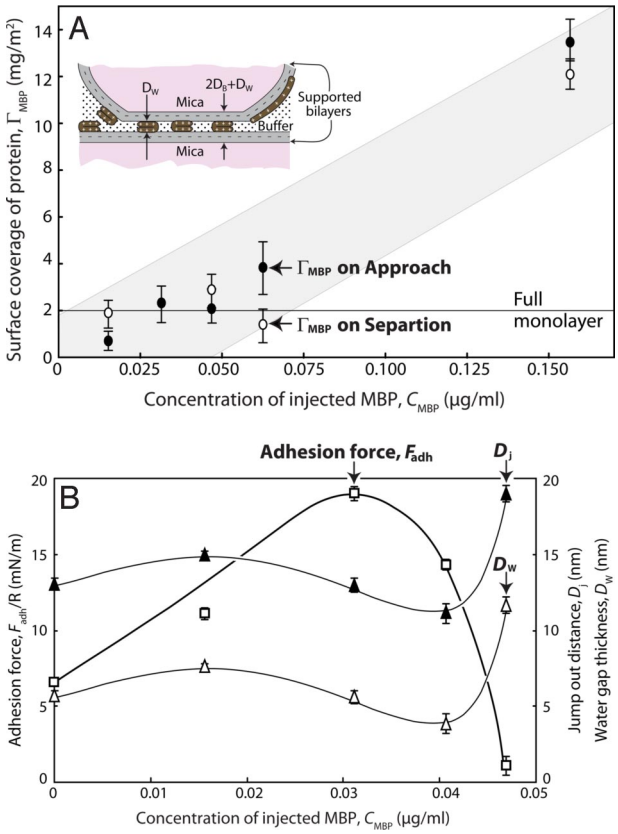

Fig. 3. Adsorbed density of MBP and adhesion forces with different amounts of MBP in solution. Calculations and measurements of injected MBP. (*A*) Calculated surface coverage of MBP (Γ_{MBP}) adsorbed between and bridging 2 cytoplasmic EAE bilayers at increasing amounts, C_{MBP}, of MBP injected into the 80-mL Mops buffer solution at pH 7.2 and 24 °C. Full monolayer coverage of MBP is shown by the line at 2 mg/m^2 estimated from Eq. **6** by using $\phi_{MBP} = 1$ and $D = 3$ nm, which corresponds to the thickness of C-shaped MBP (14). This coverage agrees with the measured Γ_{MBP} at the maximum adhesion force and minimum water-gap thickness (see *B*). (*B*) Adhesion forces measured, corresponding jump-out distances [D_j (which equals $2D_B + D_I + D_P$)], and water-gap thicknesses [D_W (which equals $D_I + D_P$)] at $C_{MBP} \leq 0.047$ μg/mL]. Note that F_{adh}/R first increases and then decreases to zero after showing a maximum at $\Gamma_{MBP} \approx 2$ mg/m^2, whereas D_j and D_W pass through a minimum close to where the adhesion is maximum. Black and white symbols refer to values measured on approach and separation (shown in Fig. 3*A*). The *Inset* in *A* is a sketch of the adsorbed bilayers showing how MBP most likely acts to couple the 2 bilayers together. Note that the absorption or surface coverage in *A* may not be linear with the MBP concentration because MBP can grow as a gel layer on the surfaces (see Fig. 5). Most likely, the adsorption has 2 regimes, one to a full, close-packed MBP monolayer (as in *A*) and the other corresponding to the growth of a gel layer.

In the presence of MBP ($\phi_{MBP} > 0$):

$$n^2(D) = (1 - \phi_B - \phi_{MBP})n_w^2 + \phi_B n_B^2 + \phi_{MBP} n_{MBP}^2,$$

i.e.,

$$\phi_{MBP} = \frac{n^2(D) - \phi_B n_B^2 - (1 - \phi_B)n_w^2}{n_{MBP}^2 - n_w^2}. \quad [5]$$

Assuming that the bilayer thickness, D_B, and hence ϕ_B, do not change on addition of MBP and during compression, ϕ_{MBP} can be readily obtained from Eq. **5** by using measurements of $n^2(D)$ and also assuming that the refractive index of the protein is known. Here, we assume $n_{MBP} \approx 1.55$ (20, 21). Finally, the surface coverage of MBP trapped between the surfaces, Γ_{MBP}, can be estimated from ϕ_{MBP} as (18)

$$\Gamma_{MBP} = \frac{1}{2}\rho_{MBP} D \phi_{MBP}, \quad [6]$$

in terms of the known density ρ_{MBP} ($\approx$1.38 g/cm^3) (22).

Fig. 3 shows the measured surface coverage of MBP (Γ_{MBP}) between the 2 surfaces at the different bulk MBP concentrations tested. On correlating the data of Figs. 2 and 3, we find that as the bulk MBP concentration increases, the adhesion initially increases, then decreases. Simultaneously, the equilibrium spacing initially decreases, then increases. Significantly, maximum adhesion occurs when the equilibrium separation is the least (green and turquoise circles in Fig. 2), i.e., when the membranes are in their most tightly packed configuration at a separation of $\approx$12 nm. At MBP concentrations >0.041 μg/mL, where the surface coverage exceeds some critical "saturation" value, the adhesion disappears, and the magnitude and range of the repulsion increases precipitously.

At MBP concentrations below the saturation value ($C_{MBP} <$ 0.041 μg/mL), quantitative analysis of the repulsive forces on

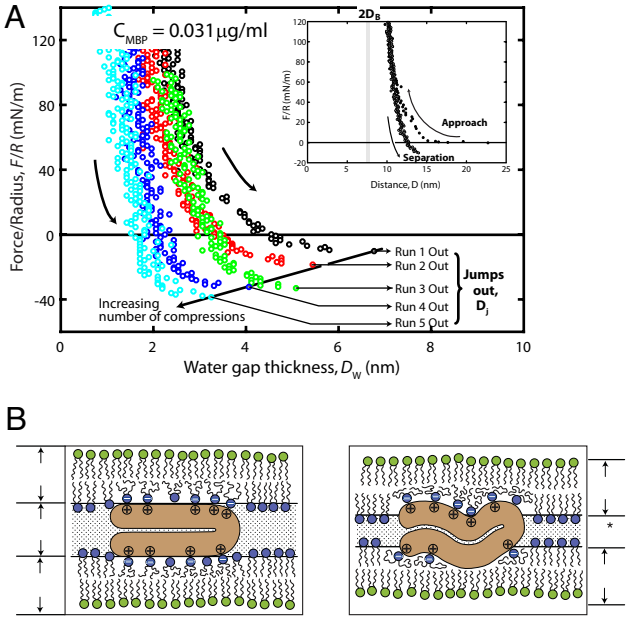

Fig. 4. Effect of previous contacts and contact time on adhesion. (*A*) Adhesion forces measured on separation in C_{mbp} 0.031 μg/mL MBP solution under the same conditions as in Fig. 2*B*. Successive force runs show a progressively increasing adhesion and a concomitant decrease of the equilibrium (contact) separation brought about by a decreasing range of the stabilizing repulsive steric force. Water-gap thickness, D_W, was obtained by subtracting $2D_B \approx 7.4$ nm from the final contact separations. The contact time in each cycle was <1 min except in cycle 3, where the 2 surfaces were kept in contact for 30 min. Note the linear relationship between the adhesion forces, F_{adh}/R, and the jump-out distances, D_j, except for the noticeable deviation in run 3. *Inset* shows the total force cycle measured on approach and separation (compare Fig. 2) and the hysteresis in the forces (compare Fig. 5). A band of $2D_B$ from 7.4–8.5 nm indicates a range of 2 bilayer thicknesses obtained by assuming a constant bilayer thickness and by subtracting a typical water-layer thickness (≈2 nm) from the final contact separation. (*B*) Possible model for the molecular rearrangements occurring on successive compressions that force the MBP molecules to penetrate deeper into the bilayers and enhance their hydrophobic contacts (15, 28). Note that MBP penetrates deeper into the bilayers with each successive compression. This mechanism would explain the decreasing range of the repulsion and the increasing adhesion. Note that D^*_W becomes less than D_W after successive compressions whereas D_B remains unchanged under the applied pressure range (<1 MPa).

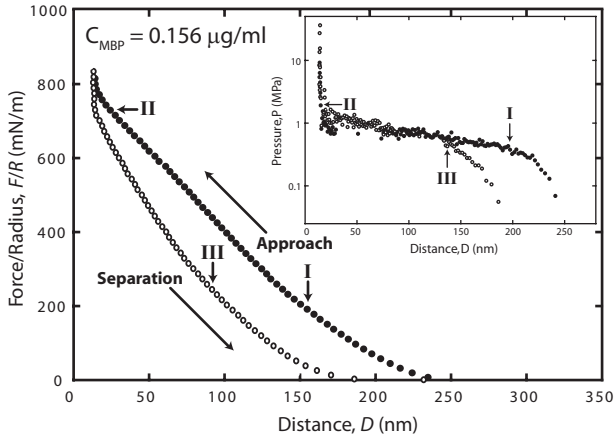

Fig. 5. Hysteretic forces in *F*/*R* vs. *D* runs measured in C_{MBP} = 0.156 μg/ml MBP solution. (*Inset*) When the force *F*/*R* between the 2 curved surfaces is converted to the pressure *P* between 2 planar surfaces (using the Derjaguin approximation to obtain *E*, then differentiating to get $P = dE/dD$), and the calculated pressure vs. distance (proportional to the water gap volume) between 2 planar surfaces is plotted, the MBP behaves like a weak gel with a collapse pressure of $P \approx 1$ MPa. The collapse resembles a first-order phase transition because it has constant (horizontal) pressure regime over a large range of D_I (water volume) corresponding to a collapse to ≈10% of the original volume occupied. The arrows indicate where the slopes of *F*/*R* and pressure change, and the corresponding letters represent the sequences from I–III.

approach (Fig. 1*A*) shows the forces to be because of the electrostatic "double-layer" repulsion between the charged surfaces: The forces are exponentially repulsive with a decay length that is close to the theoretically expected Debye length of 0.8 nm in 0.15 M $NaNO_3$ solution (straight line in Fig. 2*A*). Thus, in these near-physiological conditions, the forces are well-described by the Derjaguin–Landau–Verwey–Overbeek (DLVO) theory (23) of attractive van der Waals and repulsive electrostatic "double-layer" forces. However, in the presence of MBP, the depths of the adhesive wells are much deeper than can be accounted for by van der Waals forces acting alone, indicating that the adhesion is also because of electrostatic bridging forces [discrete ionic bonds between the negatively charged PS and lipids and the positively charged lysine or arginine amino acid (AA) groups in MBP] as illustrated in Fig. 4*B* and ref. 15. It is also noticeable that the presence of MBP brings the 2 membranes closer together than in the absence of MBP, even as MBP gets sandwiched between the 2 bilayers. At higher MBP concentrations, i.e., ≥0.047 μg/mL, there is excess MBP and, presumably, excess positive charge at the interface, which causes the bilayers to repel each other electrostatically and the water gap to swell (analogous to demyelination in vivo). But partial swelling also occurs in the absence of MBP, where $D_I + D_P$ increases by ≈2 nm (Fig. 2*B*).

Figs. 4 and 5 give further details about the effects of the number of approach–separation cycles (successive compressions and decompressions), contact time, hysteresis effects in the forces, and the likely conformations of the MBP molecules between the bilayers as a function of the coverage. We note, as has been observed in many previous force measurements between biological samples (24), that the approach is more repulsive than the separation. This effect is probably due to the initially rougher and less-correlated surfaces, which become smoothed out, where attractive species diffuse toward each other on contact to make the separation more attractive (or less repulsive). The short-range forces measured on separation are therefore likely to be closer to the "equilibrium" adhesion forces (14).

At low MBP coverage, when C_{MBP} = 0.031 μg/mL (Fig. 4*A*), there was little hysteresis in the force vs. distance curves. Fig. 4*A* further indicates that the adhesion force can be enhanced by repeated approach–separation cycles and also by increasing the equilibrium contact time between the 2 surfaces. This enhancement shows that the lipids and proteins are laterally mobile and "adaptable" and can diffuse and rearrange to find their optimum configuration (14, 25). It should be noted that the adhesive force in run 3 shows a noticeable deviation from the linear relationship shown by the straight line in Fig. 4*A*, supporting the idea that increasing the contact (equilibration) time allows the binding sites on the mobile lipid and protein molecules to find each other (24).

Another related observation is that the final contact and jump-out distances move farther in by repeated cycling. This decreasing trend in D_j suggests that the hydrophobic segments of MBP molecules penetrate into the lipid bilayers as shown schematically in Fig. 4*B*, resulting in a thinning of the membranes. Because change occurs at constant lipid and protein coverage, it suggests a deeper penetration of the MBP into the bilayers, i.e., the thinning is more of a smoothing of the membranes. Nevertheless, this process is accompanied by more water being forced out from the cytoplasmic gap, which further lowers the dielectric constant of myelin, which decreases the capacitance of the myelin sheath.

The forces are very different above the critical saturation concentration of MBP. Fig. 5 shows the very large hysteresis observed at $C_{MBP} = 0.156$ μg/mL, well above the saturation concentration of 0.041 μg/mL. The corresponding pressure–distance (or *PV* plot) between 2 planar surfaces has a shape that reveals a first-order phase transition of the MBP layer between the surfaces, suggesting that it forms a weak and/or flexible gel when present in excess (26, 27).

Analysis and Discussion of the Results. In the experiments, the mean area per lipid molecule is $a \approx 0.4$ nm^2, measured during LB depositions. This value appears to be lower than that expected for double-chain lipids and is attributed to the high amount of cholesterol present in myelin (see Table 1). The fraction of negatively charged lipids is $f \approx 0.074$, which corresponds to a negative surface-charge density of $0.4/0.074 = 5.4$ nm^2 per unit charge e^-. The estimate gives the excess number of positive charges (arginine and lysine AAs) per 18.5-kDa MBP molecule to be ≈20 (15). Thus, for full-charge neutralization each protein molecule should cover an area of $20 \times 5.4 \approx 108$ nm^2, which corresponds to a surface coverage of $\Gamma_{MBP} \approx [18{,}500/(6.02 \times 10^{23} \times 108)]$ g/nm^2 $= 0.28$ mg/m^2 per surface.[§] This value, when compared with the measured coverage of $\Gamma_{MBP} \approx 2$ mg/m^2 obtained at maximum adhesion (Fig. 3), suggests that other nonelectrostatic interactions also contribute to the adsorption.

Although the repulsive forces appear to follow the continuum theory of double-layer forces, the attractive forces do not because at the measured jump-out distances the charges on the lipid head groups and the charges on MBP must be very close to each other, if not actually in contact, so that continuum or mean field theories can no longer be used. Therefore, regarding the maximum membrane–membrane adhesion force (as mediated by MBP), assuming that at maximum adhesion every negative lipid is bound to a lysine or arginine group of MBP and that the adhesion force F/R is given by $-2\pi f\alpha\varepsilon/a$ (14, 24), where again $f \approx 0.074$ is the fraction of negatively charged lipids, $a \approx 0.4$ nm^2 is the mean area per lipid molecule, $\alpha \approx 1$ is the fraction of positive charges on MBP that are bound to the membranes, and $\varepsilon \approx 2kT$ is the Coulomb energy for an ionic bond in water (24), then the maximum F/R is calculated to be ≈9 mN/m. This value is lower than the maximum adhesion force of ≈19 mN/m measured at $C_{MBP} = 0.031$ μg/ml (Fig. 3), suggesting that other interactions such as van der Waals, hydrophobic (15, 28), hydrogen-bonding interactions (29), and weak dipolar interactions (28) also contribute to the attractive forces, which is also consistent with the structural-thickness and refractive-index changes (adsorbed MBP) observed. We note that hydrophobic- and hydrogen-bonding interactions have been shown to be important in the interactions of P0 glycoprotein in PNS myelin (29).

Finally, the MBP undergoes conformational changes when it adsorbs to the lipid bilayer (25). In the presence of excess MBP, a phase transition is observed across highly swollen bilayers, suggesting the formation of a weak, dilute, but extended gel-like structure of MBP rather than a simple electrostatic repulsion (26, 27).

We conclude that MBP maintains the structure and stability of the cytoplasmic region of the myelin sheath by acting as an electrostatic "glue" holding the negatively charged bilayers together through its positively charged amino acids groups and that hydrophobic and other attractive (adhesive) interactions are also involved. Maximum adhesion coincides with minimum water-gap thickness of the cytoplasmic space, which further implies minimum dielectric constant (or capacitance) of the myelin and, therefore, maximum transmission of nerve signals. To achieve optimum electrostatic conditions in the amounts and charge ratio (or balance) of the positive MBP and negative lipids, both must be optimized with maximum adhesion occurring at maximum densities, where each negative charge on a lipid serine head group is bound to a positive arginine or lysine group on MBP. Hydrophobic and other interactions also appear to be involved both in the adsorption and intermembrane adhesion, which are currently being investigated. Any compositional changes that lead to demyelination must also include changes to the solution, such as pH and ionic changes or addition of solutes, if these altered solutions lead to changes in the surface-charge density and/or dielectric constant that in turn affect the electrostatic and hydrophobic interactions. We do not identify the primary causes that lead to these compositional changes, only noting that these changes result in demyelination.

Removed from optimum conditions, the bilayers repel and the water gap swells, which may correspond to the onset of demyelination. This swelling can be attributed to the charge neutralization, followed by charge overcompensation, which is also common in the flocculation of colloidal particles by polyelectrolytes (30). Excess negative charge causes electrostatic swelling, but excess positive charge, i.e., excess MBP, causes swelling through the formation of a weak gel of MBP (26), possibly with some lipid (11, 26, 31) that forces the bilayers apart.[¶] This gel exhibits a phase transition on being compressed, which allows it to be collapsed when subjected to a compressive pressure of ≈1 MPa (10 atm). When the swelling pressures are not too great (e.g., 0.047 and 0.063 μg/mL in Fig. 2), the bilayers can be pressed together again to almost the same separation, within 0–2 nm, as the separation for adhesive, nonswelling systems, even from distances as large as 80 nm (Fig. 2).

These results indicate that swelling can have different causes: Excess or deficient charges on the lipid and/or MBP. For example, arginine-deficient MBP has been found to be present in some MS cases (32). To counteract the swelling, drainage of the water gap by using nontoxic hydrophilic polymers like polyethylene glycol (PEG) (33) has been successfully used to treat spinal-cord injuries in animals (34). PEG induces a high osmotic pressure (attractive depletion force) that forces the bilayers together again, perhaps collapsing the gel layer produced by unbound MBP. It also appears that there needs to be an as-yet-unknown mechanism to regulate production of MBP to match the existing surface charge in the cytoplasmic space. The insight into cytoplastic myelin bilayer interactions and swelling presented here suggests guidelines for assessing and possibly arresting or reversing myelin swelling.

Materials and Methods

Our previous work (10) identified the changes in overall lipid composition between normal (control) and EAE myelin in the white matter of the common marmoset. Previous force measurements (14) by using the mean total lipid composition of normal and EAE myelin were made in the absence and presence of an undetermined quantity of MBP. However, as shown in refs. 2 and 4, the cytoplasmic and extracellular faces of the myelin bilayer have very different compositions. We used the distributions of the lipids determined by Inouye and Kirschner (2, 4) to calculate the composition of the cytoplasmic and extracellular monolayers of the control and EAE membranes (Table 1), given the overall lipid compositions of normal and EAE myelin measured in our previous work (10). The asymmetry in lipid composition between the extracellular and cytoplasmic monolayers was believed to be the same for both control and EAE (4, 15).

Phosphatidylserine$^-$ (porcine brain PS$^-$), sphingomyelin (porcine brain SM), phosphatidylcholine (porcine brain PC), phosphatidylethanolamine (porcine brain PE), and cholesterol (ovine wool), all of purity >99%, were purchased from Avanti Polar Lipids and stored in chloroform until used. The major

[§]This estimate assumes that each protein is adsorbed fully extended on each surface as in Fig 2*A*. If the MBP bends back when bridging 2 surfaces as in Fig. 3*A*, this does not change the calculated coverage per surface.

[¶]Repulsion is also enhanced by polyunsaturated lipids through their increased repulsive undulation forces. Interestingly, EAE lipids have a greater degree of polyunsaturation than in healthy bilayers, which may also play a role in promoting demyelination (10).

chain lengths of the 3 major phospholipids (PC, PE, and PS^-) are 16:0, 18:0, 18:1, and 20:4. Dipalmitoylphosphatidylethanolamine (DPPE), sodium nitrate, calcium nitrate, and morpholinepropanesulfonic acid (Mops) sodium salt were purchased from Sigma-Aldrich. MBP was isolated from bovine-brain white matter as described (35). The MBP used was unfractionated, heterogeneous, bovine MBP.

An SFA 2000 was used for the force measurements (23, 24). The crossed-cylinder geometry of the surfaces (each cylinder of radius R) is locally equivalent to a sphere of radius R interacting with a flat surface or 2 spheres of radius $2R$. A simple geometric transformation, called the Derjaguin approximation (23), converts the force–distance curve [$F(D)$] measured between the 2 curved surfaces to the energy–distance curve, $E(D) = F(D)/2\pi R$, or pressure–distance curve, $P(D) = dE(D)/dD$, between 2 flat (planar) surfaces (23), corresponding to the interaction geometry of myelin membranes.

The lipid bilayers were deposited on the mica surfaces by using conventional Langmuir–Blodgett deposition (36). The composition used was the cytoplasmic side of EAE membranes, because MBP is found exclusively on the cytoplasmic side of the membrane. Monolayers were spread from solvent onto a pH7.2 Mops buffer (150-mN sodium nitrate/10 mM Mops sodium salt/2 mM calcium nitrate) and compressed to the desired surface pressure after solvent evaporation. As the first layer, DPPE was deposited onto the mica substrates at a surface pressure of 35 mN/m from the solid phase. The second monolayer of 23.0 mass % (37.4 mole %) cholesterol, 9.6 mass % (7.4 mole %) PS^-, 2.6 mass % (2.2 mole %) SM, 24.3 mass % (20.1 mole %) PC, and 39.0 mass % (32.9 mole %) PE was made in a 11:5:4 (vol/vol) solution of hexane/chloroform/ethanol. After the second ''myelin'' monolayer deposition at 30 mN/m onto the first DPPE monolayer, one of the bilayer-covered surfaces was transferred into the SFA chamber in buffer solution. The other surface was incubated with different amounts of MBP in buffer solution for 30 min, then rinsed twice with pure buffer solution to remove MBP molecules from the bulk and those loosely adsorbed to the surface before transferring into the SFA chamber, producing an ''asymmetric'' bilayer system consisting of a pure lipid bilayer facing an MBP-covered bilayer.

The forces F as a function of distance D were measured between the 2 curved mica-supported bilayers in solutions of varying MBP concentrations as previously described (14). The optical technique used in the measurements gave the surface radius R ($\approx$2 cm), surface separation D (to $\approx$0.1 nm), and independently the refractive indices of the various components (water, bilayer, protein) between the surfaces and hence an estimate of the in situ amounts of these components during an interaction.

ACKNOWLEDGMENTS. This work was supported by National Institutes of Health Grant R01 GM076709.

1. Raine CS (1984) in *Myelin*, ed Morell P (Plenum, New York), pp 1–41.
2. Inouye H, Kirschner DA (1988) Membrane interactions in nerve myelin. 1. Determination of surface-charge from effects of pH and ionic-strength on period. *Biophys J* 53:235–245.
3. Williams KA, Deber CM (1993) The structure and function of central nervous system myelin. *Crit Rev Clin Lab Sci* 30:29–64.
4. Inouye H, Kirschner DA (1988) Membrane interactions in nerve myelin. 2. Determination of surface-charge from biochemical data. *Biophys J* 53:247–260.
5. Jeans J (1966) in *The Mathematical Theory of Electricity and Magnetism* (Cambridge Univ Press, Cambridge, UK), pp 332–335.
6. Gilson MK, Honig BH (1986) The dielectric constant of a folded protein. *Biopolymers* 25:2097–2119.
7. Cherepanov DA, Feniouk BA, Junge W, Mulkidjanian AY (2003) Low dielectric permittivity of water at the membrane interface: Effect on the energy coupling mechanism in biological membranes. *Biophys J* 85:1307–1316.
8. Northrop RB (2001) in *Introduction to Dynamic Modeling of Neuro-Sensory Systems* (CRC, Boca Raton, FL), pp 11–12.
9. Hafler DA (2004) Multiple sclerosis. *J Clin Invest* 113:788–794.
10. Ohler B, *et al*. (2004) Role of lipid interactions in autoimmune demyelination. *Biochim Biophys Acta* 1688:10–17.
11. Riccio P, Fasano A, Borenshtein N, Bleve-Zacheo T, Kirschner DA (2000) Multilamellar packing of myelin modeled by lipid-bound MBP. *J Neurosci Res* 59:513–521.
12. Husted C (2006) Structural insight into the role of myelin basic protein in multiple sclerosis. *Proc Natl Acad Sci USA* 103:4339–4340.
13. Jo EJ, Boggs JM (1995) Aggregation of acidic lipid vesicles by myelin basic protein: Dependence on potassium concentration. *Biochemistry* 34:13705–13716.
14. Hu YF, *et al*. (2004) Synergistic interactions of lipids and myelin basic protein. *Proc Natl Acad Sci USA* 101:13466–13471.
15. Boggs JM, Moscarello MA, Papahadjopoulos D (1982) in *Lipid–Protein Interactions*, eds Jost PC, Griffith OH (Wiley, New York), pp 1–51.
16. Bates IR, Feix JB, Boggs JM, Harauz G (2004) An immunodominant epitope of myelin basic protein is an amphipathic alpha-helix. *J Biol Chem* 279:5757–5764.
17. Albersdorfer A, Feder T, Sackmann E (1997) Adhesion-induced domain formation by interplay of long-range repulsion and short-range attraction force: A model membrane study. *Biophys J* 73:245–257.
18. Raviv U, *et al*. (2002) Properties and interactions of physigrafted end-functionalized poly(ethylene glycol) layers. *Langmuir* 18:7482–7495.
19. Israelachvili J, Sammut RA, Snyder AW (1976) Birefringence and dichroism of photoreceptors. *Vision Res* 16:47–52.
20. Barer R, Tkaczyk S (1954) Refractive index of concentrated protein solutions. *Nature* 173:821–822.
21. Fisk AA (1950) The thicknesses of hemoglobin and bovine serum albumin molecules as unimolecular layers adsorbed onto films of barium stearate. *Proc Natl Acad Sci USA* 36:518–523.
22. Smith R (1982) Self-association of myelin basic protein: Enhancement by detergents and lipids. *Biochemistry* 21:2697–2701.
23. Israelachvili J (1992) in *Intermolecular and Surface Forces* (Academic, London), pp 169–250.
24. Leckband D, Israelachvili J (2001) Intermolecular forces in biology. *Q Rev Biophys* 34:105–267.
25. Mueller H, Butt HJ, Bamberg E (2000) Adsorption of membrane-associated proteins to lipid bilayers studied with an atomic force microscope: Myelin basic protein and cytochrome *c*. *J Phys Chem B* 104:4552–4559.
26. Smith R (1992) The basic protein of CNS myelin: Its structure and ligand-binding. *J Neurochem* 59:1589–1608.
27. Rapis E (2007) On the nonequilibrium phase transition in protein. *Tech Phys* 52:787–792.
28. Roux M, Nezil FA, Monck M, Bloom M (1994) Fragmentation of phospholipid bilayers by meylin basic protein. *Biochemistry* 33:307–311.
29. Luo X, *et al*. (2007) Cytoplasmic domain of zebrafish myelin protein zero: Adhesive role depends on beta-conformation. *Biophys J* 93:3515–3528.
30. Bouyer F, Robben A, Yu WL, Borkovec M (2001) Aggregation of colloidal particles in the presence of oppositely charged polyelectrolytes: Effect of surface charge heterogeneities. *Langmuir* 17:5225–5231.
31. Haas H, *et al*. (2004) Small angle X-ray scattering from lipid-bound myelin basic protein in solution. *Biophys J* 86:455–460.
32. Wood DD, Bilbao JM, Oconnors P, Moscarello MA (1996) Acute multiple sclerosis (Marburg type) is associated with developmentally immature myelin basic protein. *Ann Neurol* 40:18–24.
33. Kuhl TL, Berman AD, Hui SW, Israelachvili J (1998) Part 2. Crossover from depletion attraction to adsorption: Polyethylene glycol induced electrostatic repulsion between lipid bilayers. *Macromolecules* 31:8258–8263.
34. Borgens RB, Bohnert D (2001) Rapid recovery from spinal cord injury after subcutaneously administered polyethylene glycol. *J Neurosci Res* 66:1179–1186.
35. Cheifetz S, Moscarello MA (1985) Effect of bovine basic-protein charge microheterogeneity on protein-induced aggregation of unilamellar vesicles containing a mixture of acidic and neutral phospholipids. *Biochemistry* 24:1909–1914.
36. Zasadzinski JA, Viswanathan R, Madsen L, Garnaes J, Schwartz DK (1994) Langmuir–Blodgett films. *Science* 263:1726–1733.
37. Krigbaum WR, Hsu TS (1975) Molecular-conformation of bovine A-1 basic-protein, a coiling macromolecule in aqueous-solution. *Biochemistry* 14:2542–2546.
38. Keniry MA, Smith R (1979) Circular dichroic analysis of the secondary structure of myelin basic protein and derived peptides bound to detergents and to lipid vesicles. *Biochim Biophys Acta* 578:381–391.